Acta Cryst. (1999). A**55**, 677–682

Dynamical calculation of crystal truncation rods for surfaces and interfaces using a Cartesian coordinate transformation technique

Hung-Chun Chien,[a] Tsai-Sheng Gau,[a] Shih-Lin Chang[a]* and Yuri P. Stetsko[a,b]

[a]*Department of Physics, National Tsing Hua University, Hsinchu, Taiwan 30043, and* [b]*Chernovtsy State University, Chernovtsy 274012, Ukraine. E-mail: slchang@phys.nthu.edu.tw*

(*Received 9 July 1998; accepted 9 December 1998*)

Abstract

A dynamical calculation scheme that employs Cartesian coordinates with a z axis normal to the crystal surface to define polarization unit vectors and wavefields is applied to interpret the intensity distribution of crystal truncation rods for surfaces and interfaces. A comparison between this calculation scheme and the asymptotic iteration approach using the conventional presentation of the polarization components of the wavefields, with the σ and π components perpendicular to the wavevectors, is presented. It is found that the use of Cartesian coordinate systems can provide correct boundary conditions in determining the wavefield amplitudes, thus leading to a rigorous and general calculation scheme for dynamical diffraction from surfaces and interfaces.

1. Introduction

X-ray diffraction from surfaces, interfaces, thin films, multilayers and single-crystal bulk can be considered as general N-beam diffraction, with the integer $N \geq 0$, depending on how many reciprocal-lattice points are involved and which scan route in the reciprocal space is adopted when performing the diffraction experiment. In general, a universal theory or calculation scheme for N-beam multiple diffraction should be able to describe all the possible diffraction situations, involving either glancing-angle or wide-angle incidence or scattering. In the literature, dynamical theories and calculation algorithms for conventional wide-angle multiple diffraction, including two-beam Bragg diffraction, have been well developed (Ewald, 1937; Saccocio & Zajac, 1965*a*,*b*; Hildebrandt, 1966; Joko & Fukuhara, 1967; Ewald & Heno, 1968; Heno & Ewald, 1968; Penning & Polder, 1968; Colella, 1974; Pinsker, 1978; Juretschke, 1982; Chang, 1984; Authier *et al.*, 1996; Hung & Chang, 1989; Stepanov & Ulyanenkov, 1994). However, when a grazing angle is involved either for X-ray incidence or for scattering, the existing calculation methods (Afanas'ev & Melkonyan, 1983; Colella, 1991), though useful in some particular cases, may not be applicable to cases involving surface-normal scans (the so-called crystal truncation rods) and surface in-plane radial scans (Andrews & Cowley, 1986; Robinson, 1986; Feidenhans'l, 1989; Robinson & Tweet, 1992). Although the dynamical approach using Darwin's difference equation (Caticha, 1993, 1994; Nakatani & Takahashi, 1994) successfully describes surface-normal scans of special geometry, the generality of this approach is still limited to some special cases. Recently, an iterative technique using the minimization of the variation of the dispersion equation with respect to the eigenvalues has provided the exact values for the eigenvalues (Gau & Chang, 1995). However, the drawback of this calculation technique is that it is very time consuming in finding the correct eigenvalues. More recently, Stetsko & Chang (1997) have analysed the difficulties in dynamical calculations involving simultaneously grazing-angle and wide-angle diffraction. It has been found that under such a circumstance the off-diagonal elements of the scattering matrix are the variables of polarization, which make the dispersion equation a nonlinear equation of high-order polynomial. Thus, to find directly the solutions for eigenvalues is very difficult. If, however, a Cartesian coordinate system is chosen for the polarization unit vectors of the diffracted beams with one of the axes, say the z axis, perpendicular to the crystal surface, then the polarization-dependent variables in the off-diagonal elements can be absorbed in the eigenvectors. Thus, the dispersion equation becomes a normal eigenvalue equation, which can be solved with ease. Although it has been demonstrated that this algorithm using the Cartesian coordinates is able to handle multibeam grazing-incidence diffraction, confirmation is awaited of its effectiveness in calculating the intensity distributions of crystal truncation rods. It is the purpose of this paper to apply this Cartesian transformation technique to a surface rod and to compare the calculated results with those obtained by the iterative procedure. In the following, the algorithm using the Cartesian coordinate system will be briefly outlined for later discussion.

2. Theoretical considerations

There are two types of crystal truncation rods (or surface-normal rods) in the reciprocal space of a surface/interface: nonspecular rods with and specular rods

without the in-plane components of momentum transfer with respect to the incident wavevector. A specular rod scan is equivalent to the normal $\theta-2\theta$ scan, which can be handled by the conventional dynamical theory, while nonspecular rods are those that cause difficulties in dynamical calculation. Fig. 1 is a schematic diagram of grazing-incidence X-ray diffraction (GXID). **n** is the crystal surface normal toward the interior of the crystal, which assigns the positions of the origins of the wavevectors, the tie points, inside and outside the crystal. $\mathbf{k}_{Oi}$ and $\mathbf{k}_{Os}$ are the incident and specularly reflected wavevectors, respectively, while $\mathbf{k}_G$ and $\mathbf{k}_L$ are the diffracted wavevectors at the entrance surface of the crystal. The reciprocal-lattice points O, G and L are, respectively, the origin and the two end points of the nonspecular rod GL. The reciprocal-lattice vector **OG** of the G reflection is parallel to the crystal surface. Since the reciprocal-lattice vector **GL** is parallel to the surface normal **n**, the wavevectors $\mathbf{k}_G$ and $\mathbf{k}_L$ are identical. Points C_{Oi}, C_{Os}, C_G and C_L are the origins of the wavevectors $\mathbf{k}_{Oi}$, $\mathbf{k}_{Os}$, $\mathbf{k}_G$ and $\mathbf{k}_L$, respectively. Point A lies on **n** such that the plane of triangle AGO is parallel to the crystal surface. AO and AG are the in-plane components of $\mathbf{k}_{Oi}$ (and also $\mathbf{k}_{Os}$) and $\mathbf{k}_G$ (and also $\mathbf{k}_L$), and the angle between **AO** and **AG** is ϕ. θ_i and θ_f are the incident and the scattered angles of $\mathbf{k}_{Oi}$ and $\mathbf{k}_G$ (and also $\mathbf{k}_L$) with respect to the surface. Points $C'(j)$ are the origins of the wavevectors $\mathbf{K}_O(j)$, $\mathbf{K}_G(j)$ and $\mathbf{K}_L(j)$ (not shown in Fig. 1) inside the crystal. The z axis is along **n**. The x axis is along the OG direction and the y axis is perpendicular to the x and z axes. For the rod scan, the crystal is oriented so that θ_i and θ_f vary. There are two ways of executing the rod scan: (i) varying θ_f as θ_i is fixed, and (ii) varying θ_i and θ_f such that $\theta_i \cong \theta_f$ (Feidenhans'l, 1989; Robinson & Tweet, 1992).

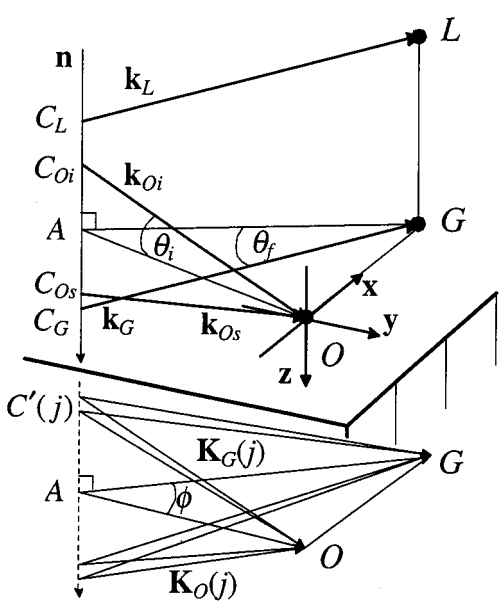

Fig. 1. Geometrical relation between the wavevectors and crystal surface in a surface-normal scan.

The intensity distribution of the nonspecular rod along GL for the two different types of scan can be calculated using the procedure given below.

According to Laue's treatment (von Laue, 1931), the fundamental equations of the wavefield in terms of the electric E fields take the form

$$2\varepsilon_M \mathbf{E}_M - \frac{(\mathbf{K}_M \cdot \mathbf{E}_M)}{k^2}\mathbf{K}_M = \sum_{M'} \chi_{M-M'}\mathbf{E}_{M'} \qquad (1)$$

for M and $M' = O$, G and L, where

$$2\varepsilon_M = (K_M^2 - k^2)/k^2 \qquad (2)$$

and $\chi_M = -[e^2\lambda^2/mc^2\pi V]F_M$. $\mathbf{E}_M$ is the electric field of the M-reflected wave. m and e are the mass and charge of the electron, V is the volume of the crystal unit cell, and F_M is the structure factor of the reflection M. $\mathbf{K}_M$ is the wavevector of the reflection M inside the crystal and $k = 1/\lambda$. Instead of adopting the conventional polarization unit vectors $\boldsymbol{\sigma}$ and $\boldsymbol{\pi}$, *i.e.* $\boldsymbol{\sigma}$ and $\boldsymbol{\pi}$ forming a mutually orthogonal system with the corresponding wavevectors **K**, we define the wavefield $\mathbf{E}_M$ in a Cartesian coordinate system as

$$\mathbf{E}_M = E_{Mx}\mathbf{x} + E_{My}\mathbf{y} + E_{Mz}\mathbf{z}, \qquad (3)$$

where **x**, **y** and **z** are the unit vectors along the x, y and z axes, respectively (Fig. 1). The components $E_{M\sigma}\boldsymbol{\sigma}_M$ and $E_{M\pi}\boldsymbol{\pi}_M$ of $\mathbf{E}_M$ in the conventional $(\boldsymbol{\sigma}, \boldsymbol{\pi})$ coordinate system (see Gau & Chang, 1995) are shown in Fig. 2(a) [the unit vectors $\boldsymbol{\pi}_M$ are parallel to the OGC' plane and $\boldsymbol{\sigma}_M = (\boldsymbol{\pi}_M \times \mathbf{K}_M)/|\boldsymbol{\pi}_M \times \mathbf{K}_M|$], while the components $E_{Mx}\mathbf{x}$, $E_{My}\mathbf{y}$ and $E_{Mz}\mathbf{z}$ in the Cartesian coordinate system are shown in Fig. 2(b). Referring to Figs. 1 and 2(b), assume that the coordinates of the tie points C' are x_n, y_n and z, where (x_n, y_n) defines the position of the surface normal **n** in the surface plane and z is a variable varying with the different modes of wave propagation, namely, $z = z_j$ for mode j. The corresponding wavevector $\mathbf{K}_M$ is then expressed as

$$\begin{aligned}\mathbf{K}_M &\equiv K_{Mx}\mathbf{x} + K_{My}\mathbf{y} + K_{Mz}\mathbf{z} \\ &= (X_M - x_n)\mathbf{x} + (Y_M - y_n)\mathbf{y} + (Z_M - z)\mathbf{z} \\ &\equiv x_M\mathbf{x} + y_M\mathbf{y} + (Z_M - z)\mathbf{z},\end{aligned}$$

where (X_M, Y_M, Z_M) is the position of the reciprocal-lattice point M.

By adopting the Cartesian coordinates for $\mathbf{K}_M$ and $\mathbf{E}_M$, the fundamental equation (1) can be written as

$$\Phi\mathbf{E} = \begin{pmatrix} (\mathbf{C}-z\mathbf{I})^2+\mathbf{B}^2-\mathbf{G}^2 & -\mathbf{AB} & -\mathbf{A}(\mathbf{C}-z\mathbf{I}) \\ -\mathbf{AB} & (\mathbf{C}-z\mathbf{I})^2+\mathbf{A}^2-\mathbf{G}^2 & -\mathbf{B}(\mathbf{C}-z\mathbf{I}) \\ -\mathbf{A}(\mathbf{C}-z\mathbf{I}) & -\mathbf{B}(\mathbf{C}-z\mathbf{I}) & \mathbf{A}^2+\mathbf{B}^2-\mathbf{G}^2 \end{pmatrix} \times \begin{pmatrix} \mathbf{E}_x \\ \mathbf{E}_y \\ \mathbf{E}_z \end{pmatrix} = 0. \quad (4)$$

For three-beam diffraction, all the matrices are 3×3 and $\mathbf{I}$ is a unit matrix. $\mathbf{A}$, $\mathbf{B}$ and $\mathbf{C}$ are diagonal matrices with the diagonal elements $a_{mm} = x_M$, $b_{mm} = y_M$ and $c_{mm} = Z_M$, respectively. The matrix $\mathbf{G}$ is defined as $\mathbf{G}^2 = k^2(\mathbf{I}+\mathbf{F})$, where the elements of $\mathbf{F}$ are given by $f_{mm'} = \chi_{M-M'}$. The vector columns of the unknown components of the electric fields are $\mathbf{E}_x = (E_{Ox}, E_{Gx}, E_{Lx})^T$, $\mathbf{E}_y = (E_{Oy}, E_{Gy}, E_{Ly})^T$ and $\mathbf{E}_z = (E_{Oz}, E_{Gz}, E_{Lz})^T$, where the superscript T means transpose. Clearly, the matrices $\mathbf{A}$, $\mathbf{B}$ and $\mathbf{C}$ are commutative.

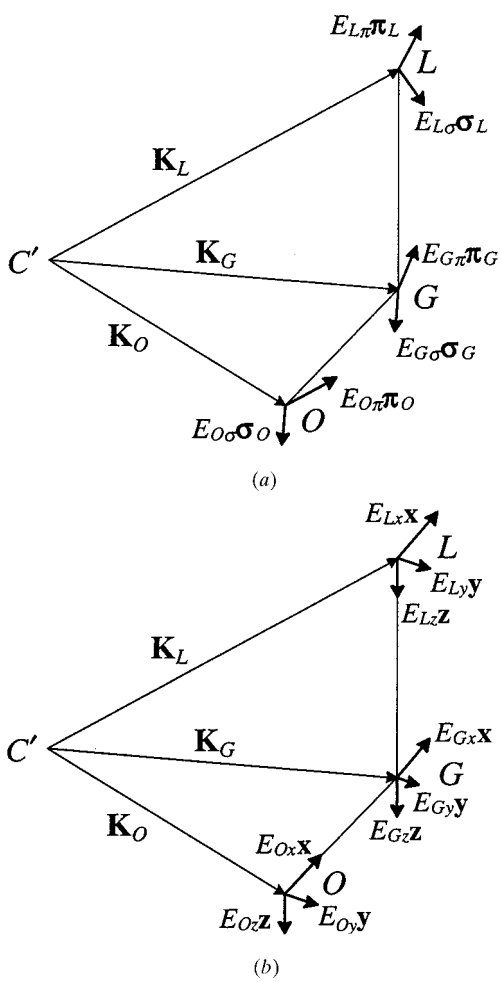

Fig. 2. The components of the $\mathbf{E}$ fields (*a*) in the $(\boldsymbol{\sigma}, \boldsymbol{\pi})$ coordinate system and (*b*) in the Cartesian coordinate system.

The unknown z can be determined from the equation of dispersion, $\det \Phi = 0$, where $\det \Phi$ is a twelfth-order polynomial.

Following the procedure given by Stetsko & Chang (1997), (4) can be reduced to an eigenvalue problem as

$$(\mathbf{Q} - z\mathbf{I}_4)\mathbf{E}_4 = 0, \quad (5a)$$

$$\mathbf{E}_z = -\mathbf{G}^{-2}(\mathbf{A}\mathbf{E}_v + \mathbf{B}\mathbf{E}_w), \quad (5b)$$

where

$$\mathbf{Q} = \begin{pmatrix} \mathbf{C} & \mathbf{0} & \mathbf{A}\mathbf{G}^{-2}\mathbf{A}-\mathbf{I} & \mathbf{A}\mathbf{G}^{-2}\mathbf{B} \\ \mathbf{0} & \mathbf{C} & \mathbf{B}\mathbf{G}^{-2}\mathbf{A} & \mathbf{B}\mathbf{G}^{-2}\mathbf{B}-\mathbf{I} \\ \mathbf{B}^2-\mathbf{G}^2 & -\mathbf{AB} & \mathbf{C} & \mathbf{0} \\ -\mathbf{AB} & \mathbf{A}^2-\mathbf{G}^2 & \mathbf{0} & \mathbf{C} \end{pmatrix} \quad (6)$$

and

$$\mathbf{E}_4 = [(\mathbf{E}_x)^T, (\mathbf{E}_y)^T, (\mathbf{E}_v)^T, (\mathbf{E}_w)^T]^T,$$
$$\mathbf{E}_v = (\mathbf{C}-z\mathbf{I})\mathbf{E}_x - \mathbf{A}\mathbf{E}_z,$$
$$\mathbf{E}_w = (\mathbf{C}-z\mathbf{I})\mathbf{E}_y - \mathbf{B}\mathbf{E}_z.$$

$\mathbf{0}$ is a zero matrix.

3. Boundary conditions for a three-beam (O, G, L) case

Equation (4) provides the amplitude ratios among the wavefields $\mathbf{E}$ for each tie point, *i.e.* for each z. The absolute amplitudes can be determined from the following boundary conditions.

(i) Continuity of the x and y components of the $\mathbf{E}$ fields at the boundary:

$$e_{Oix} + e_{Osx} = \sum_j c_j E_{Ox}(j),$$
$$e_{Gx} = \sum_j c_j E_{Gx}(j), \quad (7)$$
$$e_{Lx} = \sum_j c_j E_{Lx}(j),$$

and

$$e_{Oiy} + e_{Osy} = \sum_j c_j E_{Oy}(j),$$
$$e_{Gy} = \sum_j c_j E_{Gy}(j), \quad (8)$$
$$e_{Ly} = \sum_j c_j E_{Ly}(j),$$

respectively, where e and E are the wavefield amplitudes outside and inside the crystal, e_{Oix}, e_{Oiy} and e_{Oiz} [used in equations (9)–(11)] are the x, y and z components of the inc2ident wave, which are assumed to be unity in the calculation, e_{Osx}, e_{Osy} and e_{Osz} [used in equations (9)–(11)] are the x, y and z components of the specularly reflected wave of the O reflection, and c_j is the excitation of mode j ($j = 1, \ldots, 12$).

(ii) Continuity of the z components of the electric displacement **D** fields:

$$\begin{aligned} e_{Oiz} + e_{Osz} &= \sum_j c_j D_{Oz}(j) \\ &= \sum_j c_j [E_{Oz}(j) + \chi_O E_{Oz}(j) \\ &\quad + \chi_{O-G} E_{Gz}(j) + \chi_{O-L} E_{Lz}(j)], \\ e_{Gz} &= \sum_j c_j D_{Gz}(j) \\ &= \sum_j c_j [E_{Gz}(j) + \chi_{G-O} E_{Oz}(j) \\ &\quad + \chi_O E_{Gz}(j) + \chi_{G-L} E_{Lz}(j)], \\ e_{Lz} &= \sum_j c_j D_{Lz}(j) \\ &= \sum_j c_j [E_{Lz}(j) + \chi_{L-O} E_{Oz}(j) \\ &\quad + \chi_{L-G} E_{Gz}(j) + \chi_O E_{Lz}(j)]. \end{aligned} \tag{9}$$

(iii) Continuity of the x and y components of the magnetic induction **H**:

$$\begin{aligned} h_{Oix} + h_{Osx} &= \sum_j c_j H_{Ox}(j), \\ h_{Gx} &= \sum_j c_j H_{Gx}(j), \\ h_{Lx} &= \sum_j c_j H_{Lx}(j), \end{aligned}$$

and

$$\begin{aligned} h_{Oiy} + h_{Osy} &= \sum_j c_j H_{Oy}(j), \\ h_{Gy} &= \sum_j c_j H_{Gy}(j), \\ h_{Ly} &= \sum_j c_j H_{Ly}(j), \end{aligned}$$

respectively. Taking into account the relation $\mathbf{H}_M = (\mathbf{K}_M \times \mathbf{E}_M)/K_M$, the conditions can be expressed in terms of e and E as

$$\begin{aligned} &- e_{Oiz} y_n/k - e_{Oiy} \sin\theta_i - e_{Osz} y_n/k + e_{Osy} \sin\theta_i \\ &\quad = \sum_j c_j [K_{Oy}(j) E_{Oz}(j) - K_{Oz}(j) E_{Oy}(j)]/K_O(j), \\ &- e_{Gz} y_n/k + e_{Gy} \sin\theta_f \\ &\quad = \sum_j c_j [K_{Gy}(j) E_{Gz}(j) - K_{Gz}(j) E_{Gy}(j)]/K_G(j), \\ &- e_{Lz} y_n/k + e_{Ly} \sin\theta_f \\ &\quad = \sum_j c_j [K_{Ly}(j) E_{Lz}(j) - K_{Lz}(j) E_{Ly}(j)]/K_L(j), \end{aligned} \tag{10}$$

and

$$\begin{aligned} &e_{Oix} \sin\theta_i + e_{Oiz} x_n/k - e_{Osx} \sin\theta_i + e_{Osz} x_n/k \\ &\quad = \sum_j c_j [K_{Oz}(j) E_{Ox}(j) - K_{Ox}(j) E_{Oz}(j)]/K_O(j), \\ &- e_{Gx} \sin\theta_f - e_{Gz}(g - x_n)/k \\ &\quad = \sum_j c_j [K_{Gz}(j) E_{Gx}(j) - K_{Gx}(j) E_{Gz}(j)]/K_G(j), \\ &- e_{Lx} \sin\theta_f - e_{Lz}(g - x_n)/k \\ &\quad = \sum_j c_j [K_{Lz}(j) E_{Lx}(j) - K_{Lx}(j) E_{Lz}(j)]/K_L(j), \end{aligned} \tag{11}$$

respectively, where $g = |\mathbf{OG}|$. The coordinates of the points shown in Fig. 1 are $O(0, 0, 0)$, $G(g, 0, 0)$, $L(g, 0, -l)$, $A(x_n, y_n, 0)$, where $l = |\mathbf{GL}|$. For x_n, y_n, θ_i and θ_f, the conditions $x_n^2 + y_n^2 = k^2 \cos^2\theta_i$ and $(g - x_n)^2 + y_n^2 = k^2 \cos^2\theta_f$ hold, while for the known components e_{Oix}, e_{Oiy} and e_{Oiz} of the incident wave amplitude, the condition

$$e_{Oix} x_n/k + e_{Oiy} y_n/k - e_{Oiz} \sin\theta_i = 0$$

is satisfied. It should be noted that the angle of scattering, θ_f, can be determined as part of the self-consistent solution of the boundary conditions. However, for comparison with the experimental results, this approach is not effective. The more efficient method is to use the angles of incidence and scattering as the input and then find the appropriate eigenvalues, eigenvectors and the amplitudes through the requirements of energy and momentum conservation, as suggested here. Thereby, the calculated intensities at a given θ_f can be compared directly with the measured ones.

(iv) Continuity of the z components of the magnetic **B** fields: since the magnetic permeability μ is approximately equal to unity for X-rays, $\mathbf{B} = \mathbf{H}$. It can be easily seen that for X-rays the condition of continuity of the z components of the magnetic **B** fields follows from the condition of continuity of the x and y components of the **E** fields.

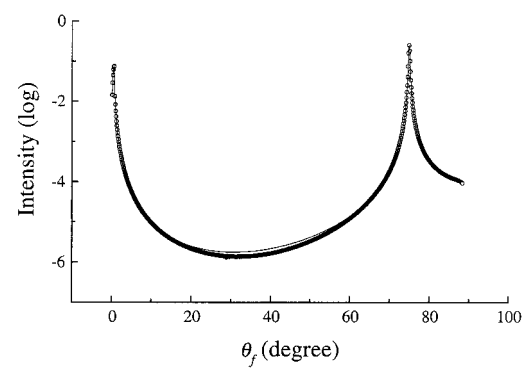

Fig. 3. Calculated intensity distributions of W(200) rod scan at $\theta_i = 0.7^\circ$ for $\lambda = 1.54056$ Å (the solid curve was calculated using the Cartesian coordinate system and the curve with open circles was calculated using the asymptotic approach).

In (7)–(11), there are 15 equations for 15 unknowns, *i.e.* $e_{Osx}, e_{Osy}, e_{Osz}, e_{Gx}, e_{Gy}, e_{Gz}, e_{Lx}, e_{Ly}, e_{Lz}$ and c_j for six (*i.e.* $j = 1, \ldots, 6$) out of the total of twelve modes for a semi-infinite crystal.

As was noted in the explanation of Fig. 1, the diffracted wavevectors $\mathbf{k}_G$ and $\mathbf{k}_L$ are equal. Consequently, these two waves are coherent. Therefore, the intensity of the rod for given θ_i and θ_f can be calculated as

$$I(\theta_i, \theta_f) = (|e_{Gx} + e_{Lx}|^2 + |e_{Gy} + e_{Ly}|^2 + |e_{Gz} + e_{Lz}|^2) \sin\theta_f \times [(|e_{Oix}|^2 + |e_{Oiy}|^2 + |e_{Oiz}|^2) \sin\theta_i]^{-1}. \quad (12)$$

4. Numerical calculations

The case under investigation here is the nonspecular rod of tungsten, (200) → (202), of Cu $K\alpha_1$, which involves three reciprocal-lattice points, (000), (200) and (202). The surface normal is along [001] and the direction [100] is parallel to the crystal surface. The structure factors used in the calculations are $F(000) = 135.904 + i11.154$, $F(200) = -96.868 - i11.154$ and $F(202) = 80.948 + i11.154$ electrons. Fig. 3 shows the diffracted intensities for this case *versus* varying θ_f, with θ_i fixed at 0.7°, calculated using both the $(\boldsymbol{\sigma}, \boldsymbol{\pi})$ coordinate system (the open circles) (Gau & Chang, 1995) and the Cartesian coordinate system (the solid line).

In general, the two calculated curves are very much alike, except for the regions of weak intensities. Since the curve of open circles is calculated by using the asymptotic approach to find the approximately correct eigenvalues, the calculated intensities are not as exact as those of the solid curve, which is obtained without approximation. The perfect match in intensity at the (200) and (202) diffraction positions is due to the fact that at the grazing incidence the diffractions at $\theta_f \cong 0$ and 76° are nearly of pure two-beam nature. The longitudinal components of **E** and **H** with respect to the wavevectors are negligibly small in the vicinity of the 200 and 202 reflections. However, this is not the case when θ_f is between 0 and 76°, because the diffraction is now of three-beam nature, involving the coupling interaction between 202 and 200, *i.e.* $202 - 200 = 002$. Moreover, the contribution of the longitudinal components of **E** and **H** to the scattered intensities becomes appreciable. This reflects that the calculated intensity using the continuous tangential components of **E** and **H** in the asymptotic approach is slightly different from that calculated with the Cartesian coordinate system.

Fig. 4 shows the intensity distributions of the same nonspecular rod when both θ_i and θ_f are varying and $\theta_i = \theta_f$ for each position. The curve with open circles is calculated using the asymptotic approach (Gau & Chang, 1995) where the boundary conditions involve only the continuous tangential components of **E** and **H** at the boundary. The solid curve is calculated using the Cartesian coordinate system. The difference between the two curves occurring at large $\theta_i = \theta_f$ angles is again due to the different boundary conditions used. The additional curve in Fig. 5 (with squares) was calculated using the components of **H** in the asymptotic approach and indicates a large deviation in intensity for lower angles and a fair match for higher angles. The discrepancy originates from the definition of the polarization unit vectors $\boldsymbol{\sigma}$ and $\boldsymbol{\pi}$ of the wavefields **E** adopted in the asymptotic approach, where $E_{M\sigma}\boldsymbol{\sigma}_M$, $E_{M\pi}\boldsymbol{\pi}_M$ and $\mathbf{K}_M$ are mutually orthogonal. This definition is, however, incorrect, because $\mathbf{E}_M$ is not necessarily perpendicular to $\mathbf{K}_M$. This discrepancy is eliminated by the use of the Cartesian coordinate system.

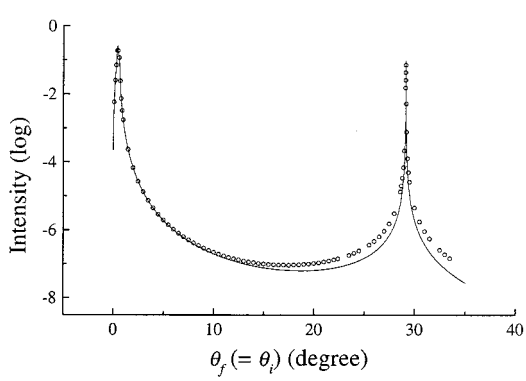

Fig. 4. Calculated intensity distributions of W(200) rod scan with varying θ_i and θ_f ($\theta_i = \theta_f$) for $\lambda = 1.54056$ Å (the solid curve was calculated using the Cartesian coordinate system and the curve with open circles was calculated using the asymptotic approach).

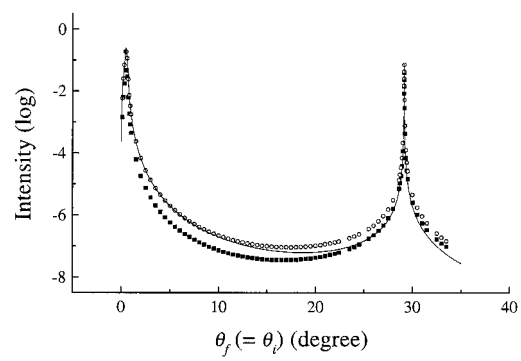

Fig. 5. Calculated intensity distributions of W(200) rod scan with varying θ_i and θ_f ($\theta_i = \theta_f$) for $\lambda = 1.54056$ Å (the solid curve was calculated using the Cartesian coordinate system, the curve with open circles was calculated using the asymptotic approach with continuous $\mathbf{E}_\parallel$ and $\mathbf{H}_\parallel$, and the curve with squares was calculated using the asymptotic approach with continuous $\mathbf{E}_\parallel$ and $\mathbf{D}_\perp$).

5. Conclusions

The calculation using the Cartesian coordinates is straightforward in finding correct eigenvalues and eigenvectors without employing any numerical iteration. On the other hand, the current approach using appropriate boundary conditions leads to a correct and easy way of calculating scattered intensities in surface/interface-related rod scans, provided that the structure of a surface/interface is known. If the atomic positions in the crystal unit cell of the surface/interface, or the moduli and phases of the structure factors are used as variables to calculate the best fit of the truncation rods to the measured ones, then this calculation scheme could, in principle, provide structural information on the surface/interface. An attempt has been made recently to analyse the interface structure of an overlayer system using the conventional dynamical theory (Gau *et al.*, 1997). However, many practical issues are yet to be clarified. Nevertheless, the calculation scheme presented here serves as a first step towards structure analysis of surfaces/interfaces using the dynamical theory.

The authors are indebted to the National Science Council for financial support. HCC, TSG and YPS are very grateful to the same organization for providing postdoctorate fellowships and a visiting scholarship during the course of this study.

References

Afanas'ev, A. M. & Melkonyan, M. K. (1983). *Acta Cryst.* A**39**, 207–210.
Andrews, S. R. & Cowley, R. A. (1986). *J. Phys. C*, **18**, 6427–6439.
Authier, A., Lagomarsino, S. & Tanner, B. K. (1996). *X-ray and Neutron Dynamical Diffraction – Theory and Applications.* New York: Plenum.
Caticha, A. (1993). *Phys. Rev. B*, **47**, 76–83.
Caticha, A. (1994). *Phys. Rev. B*, **49**, 33–38.
Chang, S. L. (1984). *Multiple Diffraction of X-rays in Crystals.* Berlin: Springer-Verlag.
Colella, R. (1974). *Acta Cryst.* A**30**, 413–423.
Colella, R. (1991). *Phys. Rev. B*, **34**, 13827–13832.
Ewald, P. P. (1937). *Z. Kristallogr.* A**97**, 1–27.
Ewald, P. P. & Heno, Y. (1968). *Acta Cryst.* A**24**, 5–15.
Feidenhans'l, R. (1989). *Surf. Sci. Rep.* **10**, 105–188.
Gau, T. S. & Chang, S. L. (1995). *Acta Cryst.* A**51**, 920–931.
Gau, T. S., Chien, H. C., Chang, S. L., Li, M. Y. & Wu, M. K. (1997). *Surf. Sci.* **384**, 254–259.
Heno, Y. & Ewald, P. P. (1968). *Acta Cryst.* A**24**, 16–24.
Hildebrandt, G. (1966). *Phys. Status Solidi*, **15**, K131–K134.
Hung, H. H. & Chang, S. L. (1989). *Acta Cryst.* A**45**, 823–833.
Joko, T. & Fukuhara, A. (1967). *J. Phys. Soc. Jpn*, **22**, 597–604.
Juretschke, H. J. (1982) *Phys. Rev. Lett.* **48**, 1487–1490.
Laue, M. von (1931). *Ergeb. Exakten Naturwiss.* **10**, 133–158.
Nakatani, S. & Takahashi, T. (1994). *Surf. Sci.* **311**, 433–439.
Penning, P. & Polder, D. (1968). *Philips Res. Rep.* **23**, 1–11.
Pinsker, Z. G. (1978). *Dynamical Scattering of X-rays in Crystals.* Berlin: Springer-Verlag.
Robinson, I. K. (1986). *Phys. Rev. B*, **33**, 3830–3836.
Robinson, I. K. & Tweet, D. J. (1992). *Rep. Prog. Phys.* **55**, 599–651.
Saccocio, E. J. & Zajac, A. (1965*a*). *Acta Cryst.* **18**, 478–480.
Saccocio, E. J. & Zajac, A. (1965*b*). *Phys. Rev. A*, **139**, 155–264.
Stepanov, S. A. & Ulyanenkov, A. P. (1994). *Acta Cryst.* A**50**, 579–585.
Stetsko, Y. P. & Chang, S. L. (1997). *Acta Cryst.* A**53**, 28–34.